High-Frequency Current Transformer Design and Construction Guide

Martin Fritsch, *Student Member, IEEE,* and Martin Wolter, *Senior Member, IEEE*

***Abstract*—High-frequency current transformers (HFCT) are well suited as sensors for measuring transient current signals on power cables, such as partial discharges (PD). If the HFCT is well designed and its measurement bandwidth matches the bandwidth of the signal to be measured, high sensitivities can be achieved. However, optimizing the HFCT design for a specific measurement bandwidth is a difficult task because various design parameters affect its transfer function. In addition, there is little helpful literature on the relationships between HFCT design and resulting sensitivity/bandwidth. To give guidance and fill this research gap, this article aims to provide all the necessary information on HFCT development. For this purpose, an analytical HFCT model is derived and validated with measurements from various self-made HFCT sensors. The method for measuring their transfer function (or transfer impedance) is presented and the measurement data of all our manufactured prototypes are given. Based on these data, valuable relationships between various design parameters and the HFCT transfer function are analyzed. Based on our experience, detailed information about the sensor manufacturing process is provided. The developed HFCT model is an effective tool to simulate and optimize the sensor transfer function before it is built. In this way, HFCT sensors can be designed quickly and cost-effectively specifically as required.**

***Index Terms*—Current transformers, current measurement, high-frequency, modeling, partial discharges, scattering parameters, simulation, transfer functions, transfer impedance**

I. Introduction

PARTIAL discharges (PD) are a first indicator of defective high-voltage insulation. Their measurement can be an effective tool for monitoring the condition of the operating assets of an electrical distribution grid. Distribution system operators therefore have a great need for cost-effective and reliable PD sensors to reduce outages and thus costs.

High-frequency current transformers (HFCT) are often recommended for measuring transient currents, such as those caused by partial discharges (PD). They are used especially for PD detection on power cables, mainly installed at the cable ends around the earth/ground connection of the cable shield or around the cable core, see Fig. 1. Due to their high sensitivity, HFCT are well suited to detect even PD of the smallest amplitude. Since the coupling between sensor and device under test is inductive and thus galvanically isolated, they are well suited for online monitoring. Furthermore, they are uncomplicated in design and easy to manufacture. All these advantages make the HFCT an excellent current sensor for the high-frequency range.

However, when we wanted to build our own HFCT to measure PD, it proved to be quite difficult. Although it is only a ferrite core with a copper winding (see Fig. 2), the choice of core material and the design of the winding have a significant impact on the final sensor performance and bandwidth. There are at least hundreds of different core materials to choose from, all with their own individual frequency response, and there is little helpful literature on basic HFCT design.

In fact, there are only a few high-quality publications that deal with this topic in detail. Ahmed [1] presents some basic considerations on the influence of the secondary winding on the HFCT bandwidth. Both Siddiqui [2] and Kluss [3] provide additional comments on the design of HFCT, the influence of different core materials, and the measurement of the transfer impedance. Both have built several prototypes for this purpose and derived valuable fundamental relationships between sensor design and sensitivity. Zachariades [4] derives similar relationships, but through simulations with a finite element model of an HFCT. Furthermore, [5] and [6] are partly related to this topic. We could not find any other peer-reviewed publications on HFCT design in the literature. To avoid misunderstandings, it should be mentioned here that all the literature on high-frequency voltage transformers for power electronics, so-called HFTs, is irrelevant to our topic. Our sensor is a current transformer (HFCT) for measuring PD on medium-voltage cables. Despite their similar name, the two devices have nothing in common.

Since there are few publications on the theory and design of HFCT sensors, there is still a lack of guidance on how to build an HFCT from scratch. Therefore, we had to do a lot of basic research on this topic to develop our own HFCT for PD measurements. After many prototypes and measurements, we finally found a design that met our requirements for maximum HFCT sensitivity at a measurement bandwidth of 10 MHz. We would like to share our results and experiences in designing HFCT to provide guidance to other scientists and engineers.

An alternative to self-made HFCT are some commercially available HFCT on the market. However, they are usually not an option because their exact frequency response cannot be adjusted and is often not sufficiently known. So, if a sensor with a custom transfer function is needed, a self-made HFCT is usually the only option. In this way, the measurement bandwidth can be selected almost arbitrarily, so that the HFCT is optimally suited for its measurement task. Furthermore, commercial HFCT are very expensive, with about $ 500–2000. Building

Manuscript received January 28, 2022; revised April 20, 2022. This paper has been written as part of the project ,,Low Cost Teilentladungsmessung" (ZS/2018/12/96267) funded by the European Regional Development Fund.

M. Fritsch and M. Wolter are with the Institute of Electric Power Systems, Otto von Guericke University, Magdeburg, D-39106 Germany (e-mail: martin.fritsch@ovgu.de, martin.wolter@ovgu.de).

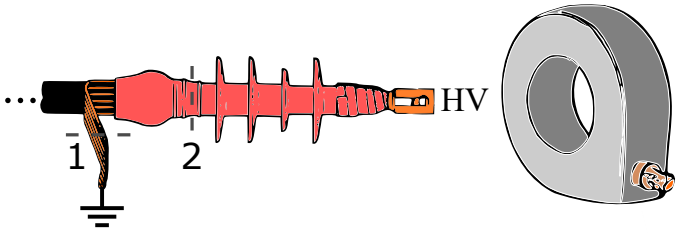

Fig. 1. Possible installation locations of an HFCT at the end of a power cable. Either around the cable shield (1), which is connected to earth/ground potential, or around the insulated part of the inner conductor (2), which is connected to high voltage (HV) potential.

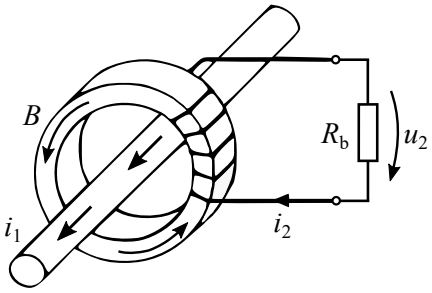

Fig. 2. Schematic representation of the operation of an HFCT sensor.

your own is much cheaper. The ferrite core costs between 20 and 50 dollars, depending on the size. The winding material and the connector only cost a few dollars. All in all, most of our HFCT prototypes were cheaper than $ 50.

This paper provides a comprehensive overview of HFCT, their design and construction. With the help of this article, anyone should be able to build an HFCT specifically designed for their measurement application. The price of the self-made sensor should be no more than one-fifth of commercial products (often much less).

Compared to previous publications, this article provides:

- An analytical model of the HFCT that is validated against measurements
- Detailed information on sensor design and guidance on core material selection
- A comprehensible method for measuring the transfer impedance of an HFCT
- The measurement results and conclusions of various self-manufactured HFCT (compared to the measurements of [3] and [4])

The article is structured as follows. The analytical HFCT model is derived in Section II. Section III shows the procedure for measuring the transfer impedance. The validation of the HFCT model can be found in Section IV. Further results are presented in Section V. Section VI provides instructions for manufacturing HFCT sensors. Finally, a conclusion is drawn in Section VII.

II. HFCT Model

An HFCT consists mainly of a toroidal core and a secondary winding around this core (see Fig. 2). The toroid is installed around an electrical conductor, such as a power cable, to measure the current i_1 flowing through it (e. g., PD pulses). This current excites a magnetic field H which is concentrated by the HFCT core (here marked by the magnetic flux density B in the core). This magnetic flux induces a voltage u_2 in the secondary winding of the HFCT which can be measured at the sensor output. To simulate the transfer function of this process, an analytical HFCT model is derived below. For HFCT, the transfer function is also referred to as the transfer impedance Z_T. In the remainder of the paper, both terms will be used.

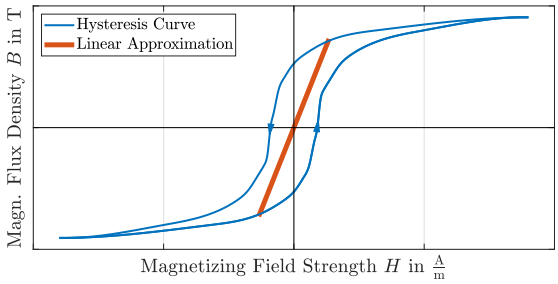

Fig. 3. Exemplary magnetization curve of a soft magnetic ferrite material at a given frequency.

In the high-frequency range, soft magnetic ferrites are predominantly used as core material. For an exemplary ferrite material, Fig. 3 shows the relationship between the magnetic flux density B in the core and the external magnetic field H (excited by the primary current i_1). This typical magnetization curve depends on the core material and the excitation frequency and is nonlinear due to hysteresis and saturation.

Because of hysteresis, we cannot write a functional relation $B = f(H)$ because the value of B at any time depends not only on H at that time, but also on its past history. However, for the soft magnetic ferrites, the hysteresis effect is quite small and negligible at this point (hysteresis losses are added to the model in a later step).

Non-linearity due to saturation occurs at high magnetic field strengths H. For typical power cables, such high fields are only to be expected at the utility frequency of 50 Hz (or 60 Hz in some countries), which is due to the power transmission in the electrical supply grid. A possible 50 Hz saturation reduces the sensitivity of the sensor over its entire bandwidth [2] [7] and is not negligible. However, the non-linear behavior of saturation is a problem in HFCT modeling, as the resulting equations cannot be solved analytically. To simplify the problem, we will split it into two parts and solve them separately. First, we assume that the 50 Hz current is zero, i.e. the HFCT core is unsaturated. Then we can develop an analytical model to simulate the HFCT transfer function. That is the content of this article. In a second step, it is planned to multiply this simulated transfer function by some kind of saturation factor to account for the effects of high 50 Hz currents. This factor depends on the level of the 50 Hz current, on the frequency, on the core material and also on possible air-gaps in the core. Thus, determining this analytical factor is a complicated task and our experiments are not yet completed. We will publish our results and how to deal with saturation in another publication as soon as possible.

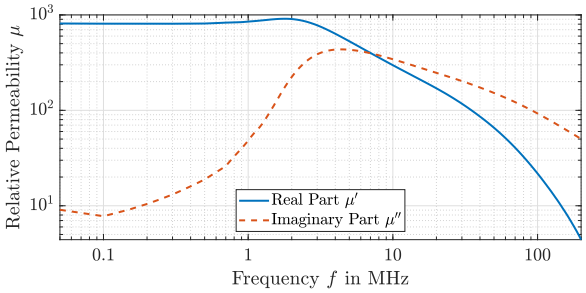

Fig. 4. Exemplary complex permeability of the material No. 43, measured and provided by the manufacturer Fair-Rite [8]. The imaginary part represents the hysteresis losses.

By neglecting hysteresis and saturation, the relationship between B and H becomes linear and depends only on material and frequency. Thus, only the linear part of the magnetization curve is processed, as indicated in Fig. 3. The proportionality factor of this linear function is the permeability $\mu'(f) = \frac{B}{H}$, which becomes constant for a given frequency (frequency dependence cannot be neglected for ferromagnetic materials). With these assumptions, it is possible to work with a frequency dependent and complex core permeability [9]:

$$\underline{\mu}_\mathrm{c}(f) = \mu'(f) - \mathrm{j}\mu''(f) \tag{1}$$

The real part μ' corresponds to the already defined permeability, i. e., the increase of the linear magnetization curve. The imaginary part μ'' describes the magnitude of the hysteresis losses caused by the oscillating magnetic field. The complex permeability $\underline{\mu}_\mathrm{c}$ of a ferrite core material can usually be obtained from the manufacturer's website. An example can be seen on Fig. 4. At low frequencies, the magnitude of the induced magnetic flux is approximately proportional to the real part of the permeability and the imaginary part is almost zero. As the frequency increases, so does the loss. The material shown has a good inductive behavior up to a frequency of several MHz. If this complex permeability of the core material is known for the frequency range of interest, the following HFCT model can be applied.

For the model, it is useful to first transform all time domain signals into the frequency domain by Fourier transformation, i. e., $i_1(t) \xrightarrow{\mathcal{F}} \underline{I}_1(f)$ and $u_2(t) \xrightarrow{\mathcal{F}} \underline{U}_2(f)$.

The basic design of an HFCT is no different from that of a conventional power transformer. Therefore, for an HFCT model the well-known equivalent circuit from Fig. 5 can be used. It consists mainly of two parts which are the primary and secondary windings on the ferrite core. Both sides are coupled by an ideal transformer with a turns ratio of $a = \frac{n_2}{n_1}$, where $n_1 = 1$. The input current $\underline{I}_1$ flowing in the primary winding induces a varying magnetic flux in the HFCT core. This behavior is represented by the magnetizing inductance $\underline{L}_\mathrm{m}$. Core losses caused by hysteresis and eddy currents are accounted for by R_fe. With ferrite materials, the eddy current losses are very small even at high frequencies due to their low conductivity [10]. The hysteresis loss is already included in the imaginary part μ'' of the complex permeability of the ferrite material. Therefore, when using ferrite toroids as the core material, R_fe can be neglected.

The magnetizing inductance is calculated as follows [11]:

$$\underline{L}_\mathrm{m}(f) = \frac{\mu_0 \underline{\mu}_\mathrm{c}(f) h_\mathrm{c} n_1^2}{2\pi} \log \frac{r_\mathrm{c,out}}{r_\mathrm{c,in}} \tag{2}$$

where h_c is the height, $r_\mathrm{c,out}$ is the outer radius and $r_\mathrm{c,in}$ is the inner radius of the core toroid in m.

R_1 and R_2 represent the resistance of the winding material which leads to thermal losses. The magnetic flux B in the core flows through all turns of the two windings. However, due to the imperfect coupling, there is also a leakage flux that does not connect all the turns. $L_{\sigma,1}$ and $L_{\sigma,2}$ account for these leakage flux losses. Since toroidal cores have a high magnetic efficiency, which means that the magnetic flux B is almost only concentrated in the ferrite core [12], the leakage flux should be very low. For the same reason, noise from electromagnetic radiation is unlikely to couple into the HFCT ferrite core. Therefore, no shielding of the final HFCT sensor is required.

The coupling via the electric field is taken into account by the parasitic capacitance C_p. This phenomenon occurs mainly at high frequencies between adjacent turns of the secondary winding. On the primary side, capacitive coupling is negligible since the primary winding consists of only a single turn $n_1 = 1$. For the same reasons, R_1 and $L_{\sigma,1}$ are close to zero and negligible. R_b is the burden or load resistance connected to the output of the HFCT. This resistance is defined by the input of a measuring device and is usually $R_\mathrm{b} = 50\,\Omega$.

The secondary winding is constructed from enameled copper wire of radius r_2 in m. One turn has the length l_2 in m. Taking the skin effect into account, the secondary winding resistance R_2 can be calculated by [13]:

$$R_2(f) = \sqrt{\frac{\omega \mu_0 \mu_\mathrm{co}}{2\sigma_\mathrm{co}}} \frac{n_2 l_2}{2\pi r_2} \tag{3}$$

where $\sigma_\mathrm{co} = 58.14 \cdot 10^6 \frac{\mathrm{S}}{\mathrm{m}}$ is the electrical conductivity of the copper conductor, $\mu_0 \approx 1.25664 \cdot 10^{-6} \frac{\mathrm{Vs}}{\mathrm{Am}}$ is the vacuum permeability, $\mu_\mathrm{co} = 1 - 6.4 \cdot 10^{-6} \approx 1$ is the relative permeability of copper and $\omega = 2\pi f$ is the angular frequency in $\frac{\mathrm{rad}}{\mathrm{s}}$. It will be shown in Section V that usually only a few secondary turns are required for a highly sensitive HFCT, so in most cases $n_2 \leq 5$. Thus, for the high-frequency range considered here, $R_2 \ll R_\mathrm{b}$ is valid and R_2 is negligible.

For simplicity, it is common to transfer the remaining elements of the secondary side to the primary side. For this, the passive elements are divided by the squared turns ratio:

$$R'_\mathrm{b} = \frac{R_\mathrm{b}}{a^2}\,, \quad L'_{\sigma,2} = \frac{L_{\sigma,2}}{a^2}\,, \quad C'_\mathrm{p} = \frac{C_\mathrm{p}}{a^2} \tag{4}$$

The resulting simplified equivalent circuit of an HFCT is shown in Fig. 6. To determine the transfer function of the HFCT, the impedances of the inductive and capacitive elements must first be calculated:

$$\underline{Z}_\mathrm{m}(f) = \mathrm{j}\omega \underline{L}_\mathrm{m}(f) \tag{5}$$

$$\underline{Z}'_{\sigma,2}(f) = \mathrm{j}\omega L'_{\sigma,2} \tag{6}$$

$$\underline{Z}'_\mathrm{p}(f) = -\mathrm{j}\frac{1}{\omega C'_\mathrm{p}} \tag{7}$$

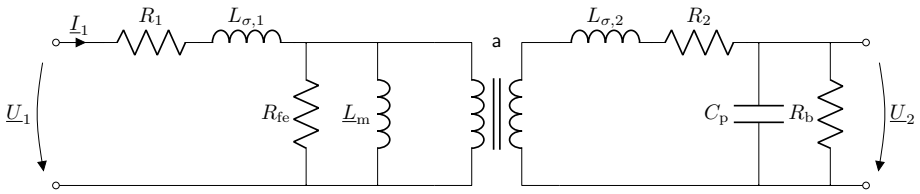

Fig. 5. Equivalent circuit of an HFCT in the frequency domain.

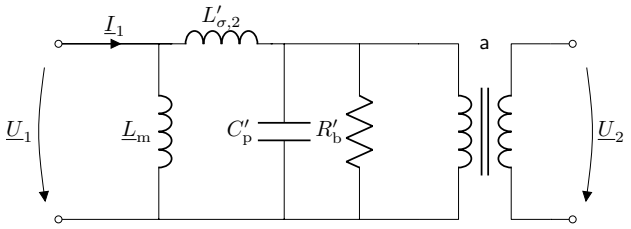

Fig. 6. Simplified equivalent circuit of an HFCT with secondary parameters referred to the primary side.

Now, the impedance of the secondary side $\underline{Z}_2$ can be summarized:

$$\underline{Z}_2(f) = \frac{R'_{\mathrm{b}} \cdot \underline{Z}'_{\mathrm{p}}(f)}{R'_{\mathrm{b}} + \underline{Z}'_{\mathrm{p}}(f)} + \underline{Z}'_{\sigma,2}(f) = \underline{Z}_{\mathrm{bp}}(f) + \underline{Z}'_{\sigma,2}(f) \quad (8)$$

Furthermore, the total impedance $\underline{Z}_{\mathrm{tot}}$ of the HFCT model is therefore:

$$\underline{Z}_{\mathrm{tot}}(f) = \frac{\underline{Z}_{\mathrm{m}}(f) \cdot \underline{Z}_2(f)}{\underline{Z}_{\mathrm{m}}(f) + \underline{Z}_2(f)} \quad (9)$$

Due to Ohm's law, the primary current $\underline{I}_1$ is:

$$\underline{I}_1(f) = \frac{\underline{U}_1(f)}{\underline{Z}_{\mathrm{tot}}(f)} \quad (10)$$

The secondary side voltage $\underline{U}_2$ can be calculated using the voltage divider rule and considering the voltage transformation ratio $\underline{U}_2(f) = \underline{U}_1(f) \cdot a$ of the ideal transformer:

$$\underline{U}_2(f) = \underline{U}_1(f) \cdot \frac{\underline{Z}_{\mathrm{bp}}(f)}{\underline{Z}_2(f)} \cdot a \quad (11)$$

Finally, with (10) and (11) the transfer impedance $\underline{Z}_{\mathrm{T}}$ of the HFCT can be calculated as follows:

$$\underline{Z}_{\mathrm{T}}(f) = \frac{\underline{U}_2(f)}{\underline{I}_1(f)} = \underline{Z}_{\mathrm{tot}}(f) \cdot \frac{\underline{Z}_{\mathrm{bp}}(f)}{\underline{Z}_2(f)} \cdot a \quad (12)$$

The transfer impedance corresponds to the sensitivity of the HFCT and indicates its ratio between input current $\underline{I}_1$ and output voltage $\underline{U}_2$. The transfer impedance is thus specified in the unit $\frac{\mathrm{V}}{\mathrm{A}}$ or Ω.

If the parasitic elements $L'_{\sigma,2}$ and C'_{p} are not known exactly, they can also be neglected and set to 0 for a simplified model (then $\underline{Z}'_{\sigma,2} \to 0$ and $\underline{Z}'_{\mathrm{p}} \to \infty$). This is probably often necessary because the parasitic elements of an HFCT are difficult to calculate or measure. Therefore, we cannot provide a generally accepted calculation method for them at this point.

TABLE I
OVERVIEW OF THE SELF-MANUFACTURED HFCT SENSOR PROTOTYPES

Inventory Number	Material	Number of Sec. Turns n_2	Core Size in mm $r_{\mathrm{c,in}} \times r_{\mathrm{c,out}} \times h_{\mathrm{c}}$
01	No. 43 NiZn	3	$35.6 \times 61.0 \times 12.7$
02	No. 43 NiZn	4	$35.6 \times 61.0 \times 12.7$
03	No. 43 NiZn	5	$35.6 \times 61.0 \times 12.7$
05	No. 78 MnZn	3	$35.6 \times 61.0 \times 12.7$
06	No. 52 NiZn	3	$35.6 \times 61.0 \times 12.7$
07	No. 43 NiZn	3	$63.5 \times 102.6 \times 15.9$
08	No. 77 MnZn	3	$35.6 \times 61.0 \times 12.7$
10	No. 43 NiZn	2	$35.6 \times 61.0 \times 12.7$
12	No. 77 MnZn	5	$35.6 \times 61.0 \times 12.7$
13	No. 52 NiZn	2	$35.6 \times 61.0 \times 12.7$
14	No. 43 NiZn	3	$23.0 \times 35.6 \times 12.7$
15	No. 52 NiZn	4	$35.6 \times 61.0 \times 12.7$

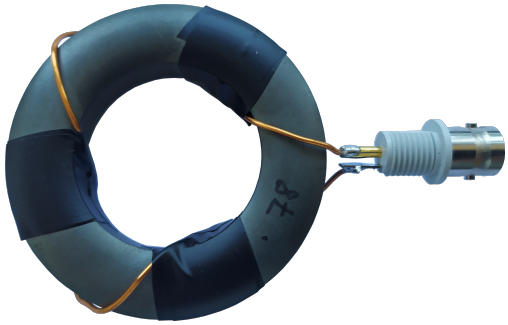

Fig. 7. Manufactured HFCT sensor with three windings on a toroidal core made of Fair-Rite's material No. 78.

In the next section, a method for measuring the transfer impedance of an HFCT is presented. Then, the model is validated using such measurements from various of our self-manufactured HFCT.

III. METHOD FOR MEASURING THE TRANSFER IMPEDANCE

We manufactured various example sensors to validate the developed HFCT model. For these prototypes, we selected different core materials and core sizes and varied the numbers of secondary turns n_2. An overview of the design parameters of the prototypes used in this work can be found in Table I. The cores were all purchased from the manufacturer Fair-Rite. An example of such a self-made HFCT sensor without housing is shown in Fig. 7.

The transfer impedance of an HFCT is best measured with a vector network analyzer (VNA). A VNA is capable of

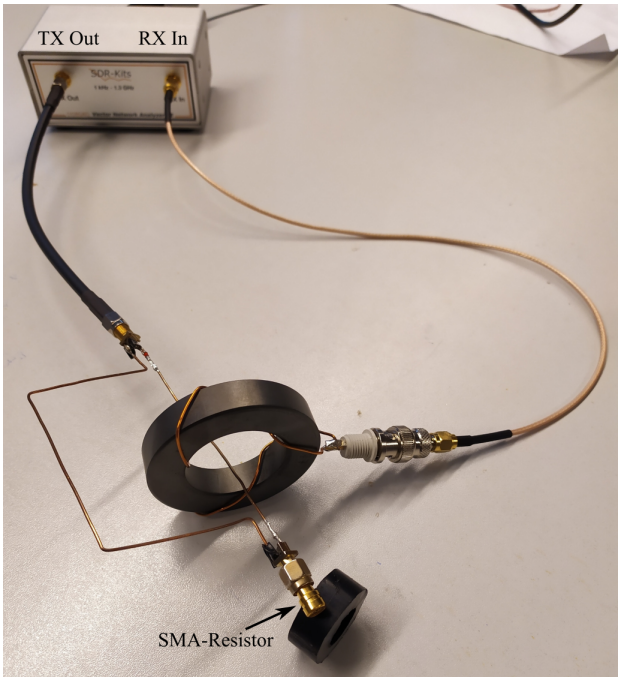

Fig. 8. Setup for measuring the transfer impedance Z_{T} of an HFCT with the help of an VNA.

measuring the scattering (S) parameters of any linear electrical network. An HFCT, like most other sensors, can be interpreted as a two-port network. Each input signal is converted into an output signal according to the sensor's transfer function. This transfer function can be calculated using the measured S parameters. The VNA used for this work is the *DG8SAQ VNWA 3E* from the manufacturer SDR-Kits. It can cover frequencies from 1 kHz to 500 MHz with a dynamic range of up to 90 dB.

For measurement, the HFCT must be connected to the VNA. For better understanding, Fig. 8 shows a picture of the measurement setup. The receive (RX) input of the VNA is connected to the output port of the HFCT. The signal from the VNA's transmit (TX) output is coupled into the HFCT via an adapter circuit. Since the connections are made with shielded coaxial cables and no measurable magnetic fields occur outside the shielding of these coaxial cables, the adapter circuit of Fig. 9 is required to couple the VNA signal into the HFCT. It is made of 1 mm thick copper wire and is used to separate the inner conductor and shield of the cable. The TX output signal of the VNA is thus unshielded inside the adapter and can be coupled into the HFCT. For this purpose, the adapter can be opened to install it around the HFCT. During the measurement, the adapter is terminated with the characteristic impedance of the coaxial cable (50 Ω) to avoid reflections on the line. The screwed-in resistor in SMA design can be seen at the bottom of Fig. 8.

To ensure that the measurement setup (cables, adapter, etc.) does not influence the actual measurement, a calibration of the entire measuring circuit must be performed. This calibration is performed with the help of the VNA software before the actual measurements begin. For better understanding of the process, part of the calibration is shown in Fig. 10. The coaxial cables and the adapter are connected to the VNA, but without

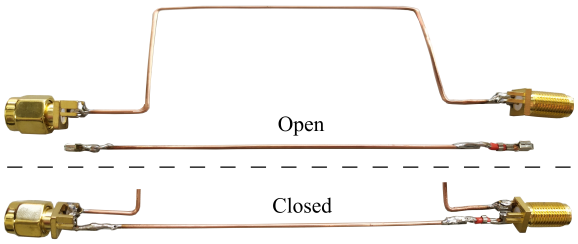

Fig. 9. Adapter for measuring the transfer impedance of an HFCT in open and closed state. The connections are pluggable.

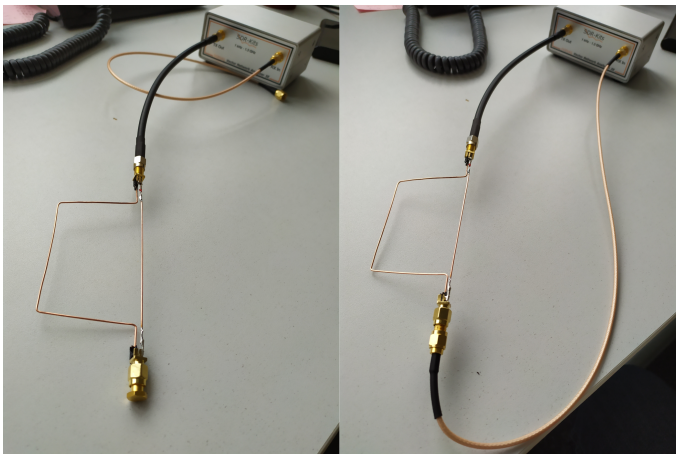

Fig. 10. Setup for calibration. Short calibration is shown on the left and Through calibration on the right.

including an HFCT. Then a SOLT-calibration (short, open, load, through) is performed with the help of the VNA software. For short-circuit, open-circuit and load calibration the TX output is terminated accordingly. For this purpose, the corresponding parts of an SMA calibration set are screwed into the end of the adapter. For the through calibration, TX and RX outputs are connected to each other. For this purpose, the output of the adapter is connected to the RX cable via an SMA female-to-female adapter. After successful calibration, the interferences of the measurement setup are compensated, so that only the HFCT behavior is measured precisely.

All measurements with the VNA are performed with a frequency sweep from 0.1 to 60 MHz to cover the entire high-frequency range. At frequencies above 60 MHz, VNA calibration could no longer be performed with sufficient quality (That is high enough since the expected signal bandwidth for PD on power cables is usually less than 10 MHz [14]). During the sweep the complex values $\underline{S}_{11}(f)$ and $\underline{S}_{21}(f)$ are measured and stored. The following equation can be used to calculate the HFCT transfer impedance:

$$Z_{\mathrm{T}}(f) = \left| \frac{\underline{S}_{21}(f) \cdot Z_{11}}{1 - \underline{S}_{11}(f)} \right| \tag{13}$$

where Z_{11} stands for the terminating impedance at the adapter. In our case the used resistor in SMA design has a resistance of $Z_{11} = 48.43\,\Omega$. This value should be measured as accurately as possible. The real value always slightly deviates from the nominal value of $50\,\Omega$.

TABLE II
MEAN DEVIATION BETWEEN SIMULATION AND MEASUREMENT

	$n_2 = 5$	$n_2 = 4$	$n_2 = 3$	$n_2 = 2$
Material No. 77	2 %	–	2 %	–
Material No. 43	4 %	5 %	7 %	9 %
Material No. 52	–	8 %	10 %	13 %

As an alternative to the VNA measurement, the HFCT transfer impedance can also be measured with a sinusoidal signal generator and oscilloscope, see for example [3]. However, such measuring methods are only suitable for low frequencies, since the measuring circuit cannot be calibrated. This means that the measurement setup falsifies the results. For example, the parasitic inductance of the adapter leads to unwanted low-pass behavior. Accordingly, the measurement results are already distorted and unusable at frequencies of a few MHz. A properly calibrated VNA measurement is therefore always preferable.

IV. MODEL VALIDATION

The developed HFCT model is validated in the following section using our self-manufactured prototypes. For this purpose, the simulated and measured transfer impedance Z_T of the HFCT are compared and presented.

Unfortunately, we were unable to accurately calculate/measure the parasitic inductance and capacitance of our HFCT prototypes. Therefore, we use the simulation results of the simplified model where $L'_{\sigma,2} = 0$ and $C'_\mathrm{p} = 0$. Accordingly, we can only validate the simplified model at the moment. We will validate the full model once we find an accurate method to determine the parasitic elements of the manufactured HFCT.

Fig. 11 shows the validation results for six selected sensors, which are a representative cross-section of all our HFCT. The blue solid lines are the measured Z_T using the method from the previous Section III. The red dashed lines are from simulations with the simplified model from Section II. For the simulations, $\underline{Z}_\mathrm{T}$ is calculated according to (12) and its magnitude is plotted.

The x-axes in Fig. 11 are limited according to the manufacturer's frequency recommendation for the respective core material. This value indicates the maximum usable bandwidth of each ferrite material. The recommended frequency for core material No. 43 is $f < 10\,\mathrm{MHz}$, for material No. 52 is $f < 20\,\mathrm{MHz}$ and for material No. 77 is $f < 1.5\,\mathrm{MHz}$ [8].

Within the recommended frequency range, the Z_T prediction of the simplified model agrees well with the measurement (see Fig. 11). For the HFCT with core material No. 77, No. 43 and No. 52, the mean deviations for different secondary winding numbers can be found in Table II (simulation overestimation in percent). A comparison of the different prototypes shows that the deviation between simulated and measured Z_T increases with decreasing secondary winding number n_2. It can also be seen that the deviation is greatest when material No. 52 is used and least when material No. 77 is used. Thus, the higher the usable bandwidth of the core material, the greater the overestimation error of the simulation. However, deviations of more than 10 % are only to be expected for $n_2 < 3$, which is probably rarely the case. For $n_2 \geq 3$, the simulation results

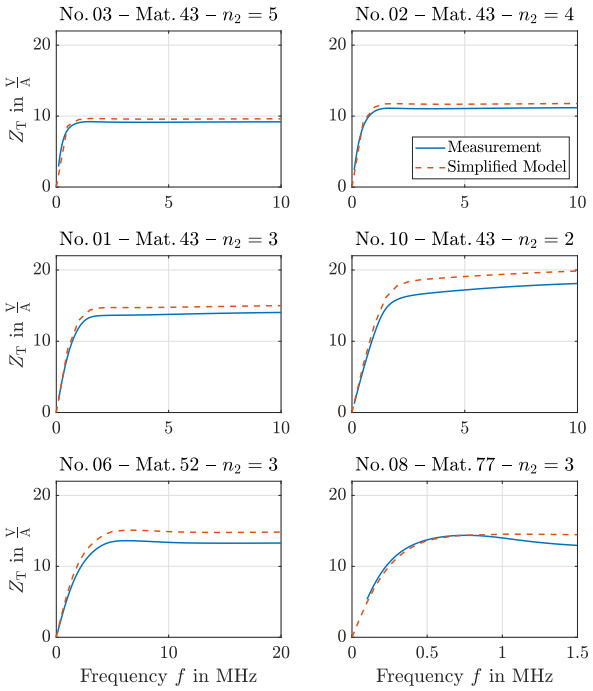

Fig. 11. Comparison of the measured and calculated transfer impedance of six exemplary HFCT prototypes. The sensors are made of three different core materials from the manufacturer Fair-Rite and have a different number of secondary turns n_2.

are close to the measured values. Accordingly, the model overestimation for most HFCT designs should be in the range of a few percent.

At higher frequencies than shown in Fig. 11, the deviation between simulation and measurement increases with frequency, but this is irrelevant since the use of the materials in these frequency ranges is not recommended anyway. Above the recommended maximum bandwidth, magnetization losses in the core increase and sensor sensitivity would decrease (see for comparison Fig. 4 for material No. 43).

The reason for the remaining deviation between simulation and measurement is due to the use of the simplified model. The two neglected parasitic parameters lead to an additional low-pass behavior. Their neglect is responsible for the remaining difference. Therefore, the simplified model overestimates the actual transfer impedance Z_T by a few percent. With this in mind, the simplified model can predict the achievable transfer impedance of an HFCT with sufficient accuracy. The simplified model thus proves to be a useful tool in the design phase of HFCT development.

If someone is able to calculate or estimate the parasitic values $L'_{\sigma,2}$ and C'_p of their HFCT in the design phase, the full model will likely lead to even more accurate predictions. However, we cannot validate this statement at the moment.

V. PARAMETERS INFLUENCING THE HFCT SENSITIVITY

This section presents further measurements on the prototypes and derives relationships between design parameters and HFCT transfer impedance.

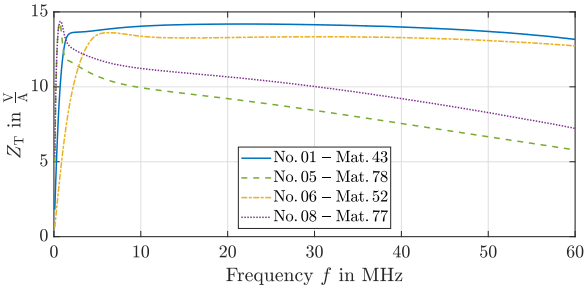

Fig. 12. Comparison of different ferrite core materials. The secondary winding number is $n_2 = 3$ for all four HFCT shown. The cores are of equal size.

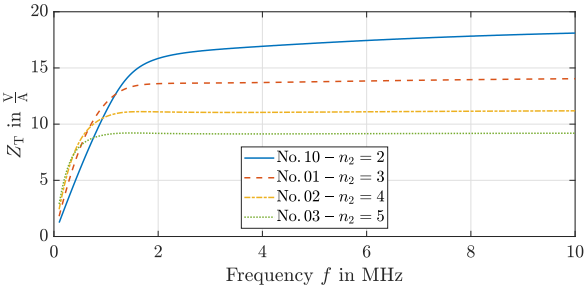

Fig. 13. Comparison of different secondary winding numbers n_2. The cores of all four HFCT are made of material No. 43 and are the same size.

First, the influence of different core materials on the transfer impedance is investigated in detail. Fig. 12 shows the measured sensitivities of sensors made of four different ferrite materials. For comparability, the secondary winding number for all four HFCT is $n_2 = 3$ and the size of their core is identical. The core material has a great influence on the bandwidth of an HFCT. Each ferrite material has its own complex permeability, which determines the frequency response of the sensor (as shown in Fig. 4). The measurement bandwidth of an HFCT is thus primarily determined by selecting the core material. Selection should be based on the manufacturer's recommended frequency range for the ferrite materials (recommended bandwidth: No. 43 for $f < 10\,\mathrm{MHz}$, No. 52 for $f < 20\,\mathrm{MHz}$, No. 77/78 for $f < 1.5\,\mathrm{MHz}$). Within the recommended bandwidth, the maximum sensitivity for all tested HFCT core materials is approximately $\hat{Z}_\mathrm{T} = 14\,\Omega$. If no recommendation is given for the bandwidth, the general rule is that the higher the initial permeability μ' at 0 Hz, the narrower the bandwidth (Mat. 52: μ'=250; Mat. 43: μ'=800; Mat. 77: μ'=2000; Mat. 78: μ'=2300) [15]. Therefore, the lower the bandwidth of the signals to be measured, the higher the permeability of the core should be. Precise information on permeability is usually available in the data sheets. Our PD sensor for power cables, for example, should be sensitive to frequencies $< 10\,\mathrm{MHz}$ [14]. Of the materials tested here, material No. 43 seems to be the most suitable for this purpose. It produces a flat frequency response of the transfer impedance over the desired frequency band.

Second, the influence of the number of turns of the secondary winding n_2 on the transfer impedance is investigated. Fig. 13 shows the measured sensitivities of four HFCT made of the same core material No. 43. Their number of secondary turns varies between two and five. The toroidal core is the same size in all four prototypes. The secondary winding number has a great influence on the sensitivity of an HFCT. It can be seen that the fewer turns the secondary winding has, the higher the maximum sensitivity of the sensor. This behavior is reasonable for current transformers because the secondary current is approximately proportional to $\frac{1}{n_2}$. On the other hand, the lower cutoff frequency increases as the number of secondary turns decreases ($n_2 = 5$: 180 kHz; $n_2 = 4$: 250 kHz; $n_2 = 3$: 400 kHz; $n_2 = 2$: 800 kHz). This means that the measurement bandwidth is reduced and the signals at the lower end of the bandwidth cannot be detected properly. Similar results were obtained by [3] and [4]. Therefore, a design that maximizes both measurement bandwidth and overall sensitivity is not possible. For each desired sensor application, the optimal secondary winding number must be determined as a compromise.

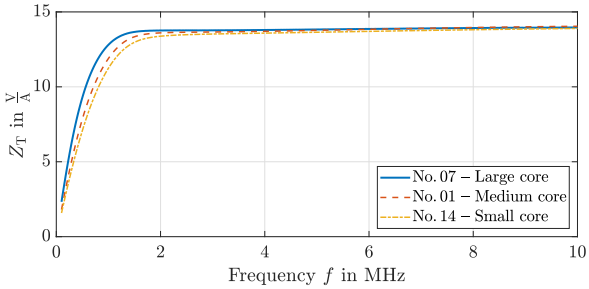

Fig. 14. Influence of core size on the transfer impedance. The secondary winding number is $n_2 = 3$ for all three HFCT shown. The cores are made of material No. 43.

Third, the effect of core size on transfer impedance is investigated. Fig. 14 shows the measured sensitivities of HFCT from three different core sizes. All three are made of material No. 43 and the secondary winding number is $n_2 = 3$. The core size has a small influence on the bandwidth of an HFCT. With a larger core, the sensitivity in the lower frequency range increases slightly, i. e., the lower cutoff frequency decreases. This means that the measurement bandwidth of the HFCT widens downward with increasing core size. But this effect is only minor. Furthermore, the core size is usually predetermined by the diameter of the power cable, so it cannot be chosen arbitrarily. Accordingly, the core size has only little effect on the transfer impedance of the sensor.

VI. Manufacture of HFCT Sensors

This section provides some general advice on building HFCT sensors based on our experience with the prototypes we built ourselves.

Since the bandwidth of an HFCT is mainly determined by its core, great attention should be paid to the selection of the material. For selection, the desired frequency range in which the sensor is to measure signals must be specified. For example, our PD sensor should have a measurement bandwidth of 10 MHz [14]. Then a suitable core material can be selected for the specified measurement bandwidth. Core manufacturers provide material overviews that can be used

for orientation. Look up the recommended frequency range for the various materials. For example, we obtained our cores from the manufacturer Fair-Rite, who provides detailed lists of available materials and their properties. Based on these lists, we selected material No. 43 for $f < 10\,\mathrm{MHz}$. In general, ferrite materials are best suited for the cores because they have low losses in the high-frequency range. Two types of ferrites are distinguished. Nickel-zinc (NiZn) ferrites are the better choice for applications with frequencies above 3 MHz. Manganese-zinc (MnZn) ferrites have higher permeabilities and are more suitable for frequencies below 3 MHz [16].

Regarding the core shape, closed toroids are the most suitable. Higher sensitivities are achieved due to the absence of air gaps in the ferrite material. A disadvantage of these closed toroidal cores is that they cannot be installed without opening the electrical circuit of the primary conductor. Here it is preferable to use split cores, which have the same sensitivity at 0 mm air gap as a closed toroidal core. When the distance between the air gaps is increased, the sensitivity of the HFCT is reduced over the entire bandwidth, which also prevents core saturation [2] [7]. Nevertheless, only closed cores are discussed in this article. We are still investigating the best way to handle possible 50 Hz saturation, the influence of air gaps, and the construction of split cores, and will report on these in a later article.

The inner diameter of the toroid core should be selected based on the outer diameter of the primary conductor. The primary conductor should fit comfortably through the core. However, the core should also not be too large, otherwise the installation will be difficult. The larger the core, the heavier and more expensive the sensor. The effect of the core size on the sensitivity is small as shown in Section V.

After the core is selected, the next step is the winding. The number of turns of the secondary winding has a great influence on the HFCT sensitivity. In general, the smaller the number of turns, the higher the overall sensitivity, but at the cost of bandwidth. Especially the lower cutoff frequency is affected by the number of secondary turns. The resulting transfer impedance can be checked with the HFCT model to find an optimum. Based on our experience, a reasonable number of turns is between 2 and 5, depending on the desired sensor application. For our exemplary PD sensor, we use three turns as a trade-off between sensitivity and bandwidth (compare to Fig. 13).

When manufacturing the winding, care should be taken to distribute the winding as evenly as possible over the core to avoid leakage flux. Enameled copper wire with a small diameter is suitable as secondary winding material. It is easy to wind and only slightly reduces the inner radius $r_{\mathrm{c,in}}$ of the core toroid. The authors use a wire with a diameter of $r_2 = 0.5\,\mathrm{mm}$. However, investigations have shown that the wire diameter has no influence on the sensor sensitivity, so it can be chosen arbitrarily [15]. Alternatively, stranded wire can be used. Although the use of stranded wires is often not recommended in the high-frequency range [17], the authors cannot confirm this for HFCT applications. When stranded wire was used, no difference in sensor transfer impedance was observed compared to solid wire, even at 60 MHz.

The connection between the secondary winding and connector should be as short as possible to avoid further parasitic inductance. A BNC or SMA connector is usually used to connect the HFCT to a measuring device.

Since uniformly wound toroidal coils are inherently immune to magnetic interference fields [12], additional shielding of the HFCT is not required.

Nevertheless, the sensor should be well suited for permanent outdoor installation. An insulating, waterproof housing should be provided for this purpose. Such a housing made of insulating material has almost no influence on the sensitivity of the sensor [3]. The housing reduces the usable inner radius $r_{\mathrm{c,in}}$ of the toroid. This should be considered when selecting the core size.

VII. Conclusion

This article explains the theory, design and construction of HFCT sensors. With its help, it should be possible for anyone to design and build an HFCT according to their individual needs.

For this purpose, an analytical HFCT model is first derived. The model is validated against measurements and can be used to simulate the transfer function of arbitrary HFCT. It is attached to the article as Matlab script. To validate this model, various sensors were manufactured and their transfer impedance was measured. The procedure for measuring the transfer impedance is explained in a comprehensible way. In addition, the measured values of 12 different HFCT are presented and the influence of core material, secondary winding number and core size on the transfer impedance is analyzed. Furthermore, the experience gained in the manufacturing process is summarized to provide guidance on how to design and build HFCT.

Since we could not accurately calculate the parasitic inductance and capacitance of our HFCT prototypes, we validated a simplified version of the model. We will validate the full model once we find an accurate method to determine these parasitic parameters. The simplified HFCT model is obtained by neglecting the parasitic parameter and was successfully validated. It makes good predictions for the transfer impedance. The results are slightly overestimated, but still sufficiently good. The model thus enables a simulative design of HFCT.

Possible saturation effects due to high 50 Hz currents are neglected in the model, as it would otherwise be non-linear and thus not analytically solvable. Therefore, the model calculates the HFCT transfer function in an unsaturated state. It is planned to multiply this simulation result afterwards with a saturation factor to account for the effects of the high 50 Hz currents. Our saturation experiments are not yet complete. How saturation will affect the final HFCT sensitivity and how to best deal with it will therefore be published in a later article.

In the end, the transfer function of an HFCT can be selected almost arbitrarily by choosing the right core material and secondary winding number. The bandwidth is mainly determined by the core material, while the number of secondary windings determines the maximum sensitivity and slightly changes the lower cutoff frequency of the sensor. Core size has almost no effect on HFCT performance.

The article is thus a comprehensive guide for anyone who wants to build their own HFCT for current measurements. This

is of interest for various researchers as well as application engineers. For example, the authors intend to design HFCT with a bandwidth of $< 10\,\mathrm{MHz}$ for PD detection. Based on the research in this article, the sensor sensitivity could be maximized within the proposed measurement bandwidth.

REFERENCES

[1] N. Ahmed and N. Srinivas, "On-line partial discharge detection in cables," *IEEE Transactions on Dielectrics and Electrical Insulation*, vol. 5, no. 2, pp. 181–188, apr 1998.

[2] B. A. Siddiqui, P. Pakonen, and P. Verho, "Novel inductive sensor solutions for on-line partial discharge and power quality monitoring," *IEEE Transactions on Dielectrics and Electrical Insulation*, vol. 24, no. 1, pp. 209–216, feb 2017.

[3] J. V. Kluss, A.-P. Elg, and C. Wingqvist, "High-frequency current transformer design and implementation considerations for wideband partial discharge applications," *IEEE Transactions on Instrumentation and Measurement*, vol. 70, pp. 1–9, 2021.

[4] C. Zachariades, R. Shuttleworth, R. Giussani, and R. MacKinlay, "Optimization of a high-frequency current transformer sensor for partial discharge detection using finite-element analysis," *IEEE Sensors Journal*, vol. 16, no. 20, pp. 7526–7533, oct 2016.

[5] A. Rodrigo, P. Llovera, V. Fuster, and A. Quijano, "Study of partial discharge charge evaluation and the associated uncertainty by means of high frequency current transformers," *IEEE Transactions on Dielectrics and Electrical Insulation*, vol. 19, no. 2, pp. 434–442, apr 2012.

[6] F. Álvarez, F. Garnacho, J. Ortego, and M. Sánchez-Urán, "Application of HFCT and UHF sensors in on-line partial discharge measurements for insulation diagnosis of high voltage equipment," *Sensors*, vol. 15, no. 4, pp. 7360–7387, mar 2015.

[7] M. J. Foxall, A. P. Duffy, J. Gow, M. Seltzer-Grant, and L. Renforth, "Development of a new high current, hybrid 'ferrite-rogowski', high frequency current transformer for partial discharge sensing in medium and high voltage cabling," in *59th International Wire & Cable Symposium*, Rhode Island Convention Centre, Providence, RI, USA, Nov. 2010.

[8] Material Data Sheets. (2021, Jun.) Fair-Rite Products Corp. homepage. [Online], available: https://www.fair-rite.com/materials/.

[9] M. Getzlaff, *Fundamentals of Magnetism*. Springer Berlin Heidelberg, 2010, pp. 139–141.

[10] N. A. Spaldin, *Magnetic Materials*. Cambridge University Press, 2014, pp. 120-125.

[11] W. H. Hayt and J. A. Buck, *Engineering electromagnetics*, 6th ed., ser. McGraw-Hill series in electrical engineering. Boston, Mass. [u.a.]: McGraw-Hill, 2001, pp. 263-264.

[12] D. J. Griffiths, *Introduction to Electrodynamics*. Cambridge University Press, 2017, pp. 247-250.

[13] M. Fritsch and M. Wolter, "Transmission model of partial discharges on medium voltage cables," *IEEE Transactions on Power Delivery*, 2021, to be published.

[14] M. Fritsch and M. Wolter, "Measurable bandwidth of partial discharges on medium voltage cables," in *2021 IEEE PES General Meeting (PESGM)*. IEEE, Jul. 2021, accepted paper.

[15] J. V. Kluss and A.-P. Elg, "Challenges associated with implementation of HFCTs for partial discharge measurements," in *2020 Conference on Precision Electromagnetic Measurements (CPEM)*. IEEE, Jul. 2020.

[16] Learn More About Ferrite Cores. (2021, Jun.) Magnetics homepage. [Online], available: https://www.mag-inc.com/Products/Ferrite-Cores/Learn-More-about-Ferrite-Cores.

[17] R. P. Wojda, "Winding resistance and power loss for inductors with litz and solid-round wires," in *2016 IEEE International Power Electronics and Motion Control Conference (PEMC)*. IEEE, sep 2016.

Martin Fritsch (S'20) was born in Muehlhausen, Germany in 1993. He received his B.Eng. from the Frankfurt University of Applied Science in 2016 and his M.Sc. from the Otto von Guericke University Magdeburg (OVGU), Germany in 2018, both in electrical engineering.
He is currently working as a Research Assistant at the Chair of Electric Power Networks and Renewable Energy at the OVGU. His research interests include the modeling of electric power systems and the detection of partial discharges.

Martin Wolter (S'06, M'08, SM'16) was born in Hannover, Germany in 1981. He received his diploma degree in 2006, his Ph.D in 2008 and his venia legendi in 2012 all from Leibniz University Hannover, Germany.
He was Head of the System Operation Concept Development Team at 50 Hertz Transmission GmbH, for four years. Since 2015 he is Head of the Chair Electric Power Networks and Renewable Energy at the Otto von Guericke University Magdeburg, Germany. His research interests are modeling and simulation of interconnected electric power systems, development of planning and operation strategies and multi-agent systems.